



Supplementary Materials for

Programmable on-chip DNA compartments as artificial cells

Eyal Karzbrun, Alexandra M. Tayar, Vincent Noireaux, Roy H. Bar-Ziv*

*Corresponding author. E-mail: roy.bar-ziv@weizmann.ac.il

Published 15 August 2014, *Science* **345**, 829 (2014)
DOI: 10.1126/science.1255550

This PDF file includes:

Materials and Methods
Supplementary Text
Figs. S1 to S16
Tables S1 to S3
References

Other Supplementary Material for this manuscript includes the following:

available at www.sciencemag.org/content/345/6198/829/suppl/DC1

Movies S1 and S2

MATERIALS AND METHODS	3
DNA CONSTRUCTS.....	3
BIOCHIP PREPARATION.....	3
IMAGING.....	6
DNA BRUSH.....	6
THE ENDOGENOUS E. COLI CELL-FREE EXTRACT.....	6
CALIBRATION OF GFP CONCENTRATION AND DIFFUSION.....	7
EXPRESSION DYNAMICS VARIATION.....	8
PROTEASE ACTIVITY IN THE DNA COMPARTMENT.....	8
SUPPLEMENTARY TEXT	9
SINGLE COMPARTMENT THEORY: THE EFFECTIVE LIFETIME.....	9
SINGLE COMPARTMENT THEORY: GENE EXPRESSION ONSET TIME.....	10
ONE-DIMENSIONAL ARRAY OF CONNECTED COMPARTMENTS: EXPRESSION AND DIFFUSION.....	11
ONE-DIMENSIONAL ARRAY OF CONNECTED COMPARTMENTS: FLOW CONSIDERATIONS.....	13
REFERENCES	14
FIG. S1. MICROFLUIDIC DEVICE AND THE DNA COMPARTMENT	16
FIG. S2. FABRICATION AND ASSEMBLY OF THE MICROFLUIDIC DEVICE	17
FIG. S3. SEM MEASUREMENT OF THE SILICON DEVICE	18
FIG. S4. GFP CALIBRATION AND DIFFUSION INTO THE COMPARTMENTS	19
FIG. S5. KINETICS AND LINEAR PROFILE OF GFP	20
FIG. S6. ACTIVATOR AND REPRESSOR DETAILED NETWORK SCHEME	21
FIG. S7. GFP EXPRESSION ONSET TIME	22
FIG. S8. GFP PROFILE SLOPE	23
FIG. S9. VARIATION BETWEEN COMPARTMENTS	24
FIG. S10. VARIATION BETWEEN COMPARTMENTS FOR NEGATIVE FEEDBACK CONSTRUCT	25
FIG. S11. OSCILLATORY NETWORKS	26
FIG. S12. ACTIVATOR AND REPRESSOR PULSE DYNAMICS	27
FIG. S13. PROTEIN DEGRADATION BY CLPXP	28
FIG. S14. COMMUNICATION BETWEEN CONNECTED DNA COMPARTMENTS	29
FIG. S15. COMMUNICATION BETWEEN CONNECTED DNA COMPARTMENTS FOR GENES PATTERNED IN REVERSE ORDER	30
FIG. S16. ONE-DIMENSIONAL ARRAY OF CONNECTED COMPARTMENTS	31
TABLE S1. DNA MODULES	32
TABLE S2. DNA CONSTRUCTS – SINGLE GENE	33
TABLE S3. DNA CONSTRUCTS – ACTIVATOR-REPRESSOR NETWORKS	34
MOVIE S1	35
MOVIE S2	35

Materials and Methods

DNA Constructs

DNA parts used in this work are described in table S1. Their assembly into single gene constructs and two gene networks are described in tables S2 and S3, respectively as well as in figure S4. All the plasmids were constructed from the pBEST-Luc plasmid (Promega), with the UTR1 (untranslated region), except for the pBAD plasmid (araBAD promoter).

Biochip Preparation

We review the fabrication and assembly process of the DNA compartments in a microfluidic device. Each step is detailed in a subsection and illustrated in Figure S2.

Design of the device

The device consisted of 84 circular wells (compartments), etched 2 – 3 μm deep into a silicon wafer (Fig. S1). Silicon wafers (5", 0.525mm thickness, test grade, <100>, p-type, University Wafers, Boston, MA) were used as the substrates. Each compartment had a diameter of 100 μm and was connected through a 20 μm wide and 50 – 300 μm long capillary channel to a perpendicular flow channel, 30 – 40 μm deep and 300 μm wide. At one end of the flow channel there was an inlet – a circular chamber, etched 30 – 40 μm deep and 2mm in diameter. At the other end, the flow channel was connected to a 100 μm serpentine that ends at an outlet - a circular chamber, etched 30 – 40 μm deep and 2mm in diameter.

Step 1: Etching

Resist Coating

S1818 or S1813 photoresist (MicroChem, Newton, MA) was applied by a spin-coater (model PWM32, Headway Research Inc., Garland, TX) onto each wafer in a single step process: 2000 rpm for 40 sec with a ramp of 1000 rpm/s. The resists were pre-baked for 1 minute at 115°.

Lithography

Using a mask aligner (6mW/cm², Karl Suss MA6/BA6, Garching, Germany), the samples were exposed for 40 seconds, through a polyester based photomask (CAD/Art Services Inc. Bandon, OR). Each mask contained six devices.

Post exposure bake

The samples were post-developed for 40 sec in MF319 and rinsed with water. The resulting resist thickness was 1.8 μm for S1813 and 2.8 μm for S1818.

Reactive Ion Etching (RIE)

An Advanced Silicon Etch ICP-RIE (Surface Technology Systems, New Port, England) was used for etching. The 2 μm height features were etched using the following parameters for 40 seconds: pressure of 30mT, SF6 flow rate of 130sccm, O2 flow rate of

13sccm, power of 500W applied to the 13.56 MHz RF coil and 100W to the platen. For the 40 μ m deep features we used a protocol based on the Bosch protocol (23) with an alternating passivation/etching process. Etching parameters were: pressure of 30mT, SF6 flow rate of 130sccm, O2 flow rate of 13sccm, power of 500W applied to the RF coil and 100W to the platen. Passivation parameters were: pressure of 30mT, C4F8 flow rate of 30sccm and a power of 500W applied to the coil. Each step was 10 sec in duration and total etching process was 20 cycles.

After etching, the samples were rinsed in acetone and isopropanol to remove any remaining photoresist. A SEM image of the device is presented in Figure S3. The fabricated silicon wafers were cut into six devices, 24x48 mm² each, using a diamond-head scribe and manually breaking of the wafer.

Step 2: Inlet and outlet drilling

Holes were drilled to form an inlet and an outlet in the device. We used a bench drill machine (Proxxon, TBM 220) and a Dremel 7103 diamond wheel point drill. The holes were drilled through the circular etched inlet and outlet at the ends of the flow channel. The device was cleaned following drilling: boiling in ethanol at 70°C for 10 minutes followed by sonication and cleaning with basic piranha solution (H₂O₂:NH₃:H₂O; 1:1:4, heated to 70°C for 10 minutes) and dried using Argon.

Step 3: SiO₂ Coating

The device was coated with a ~50nm SiO₂ layer deposited by low-temperature atomic layer deposition (FIJI F200, Cambridge Nanotech).

Step 4: Biocompatible Photoactivable Monolayer Assembly

The SiO₂ coated device was incubated with a polymer solution. The polymer was composed of a polyethylene glycol backbone with a Nvoc-protected amine at one end, and a trialkoxysilane function at the other end (16). The polymer concentration was 0.2 mg/ml in Toluene and the incubation process was 10-20 min during which a monolayer was formed on the surface. The incubation was followed by washing in Toluene and drying.

Step 5: Lithography patterning

The lithography process was performed by placing the fabricated chip on a translational stage coupled to an inverted microscope (Zeiss Axiovert 200). UV light from fluorescent light source (EXFO X-Cite 120Q), was passed through a rectangular pinhole and a 365nm band pass filter (Chroma) and focused on the substrate with a X60 objective. The exposure time was set to yield a total 2.5 Joule/cm² (16). The areas on the surface that were exposed to UV light were de-protected and an amine group was exposed.

Step 6: Biotin coating.

Biotin N-hydroxysuccinimidyl ester (biotin-NHS) dissolved in a borate buffered saline (0.5 mg/ml) was incubated on the chip for 15 minutes. The biotin-NHS covalently bound

to the exposed amine groups on the UV exposed monolayer. We thus attained a surface patterned with biotin.

Step 7: DNA deposition and brush assembly.

Linear DNA fragments were produced by polymerase chain reaction (PCR) with KAPA HiFi HotStart ReadyMix (KK2601, KAPA BIOSYSTEMS), using one primer with biotin and another with Alexa Fluor 647, both attached at the 5'-end (IDT). The biotin primer was located downstream to the transcription terminator. PCR products were cleaned twice using Promega Wizard® SV-Gel and PCR Clean-Up. DNA was conjugated to streptavidin (SA) by mixing in solution in a molar ratio of 1:1.5 DNA:SA. The final DNA solution contained SA conjugated DNA at a concentration of 100 – 300nM in a phosphate buffered saline.

Nano-liter DNA-SA droplets were individually deposited onto the reactor chambers using the GIX Microplotter II (Sonoplot Inc., Middleton, WI) and 60 μ m diameter micropipettes. The DNA-SA solutions were incubated on the device for an hour in a PBS buffer. During incubation the DNA formed a dense brush on the surface. The brush density was of the order of 10³ DNA μ m⁻². The promoter orientation of the DNA was toward the surface of the brush. Finally, DNA brushes were localized to the UV patterned areas inside the etched compartments (Fig. 1).

The device was then bathed in PBS and then in water to remove excess adsorbed DNA. The device was carefully removed from the water bath. The hydrophobicity of the monolayer coating left a dry surface, except where DNA brushes formed

Step 8: Sealing the device

The device front side (the fabricated side) was sealed with a PDMS coated coverslip and magnets. Magnets embedded in a punched PDMS were attached to the backside of the device (the untreated side of the device), aligned to the drilled inlet and outlet. At this point the device was dry.

Step 9: Flowing the cell-free extract.

The device inlet was connected using microfluidic tubing to a reservoir of PBS cooled to 4°C with a cooling circulator (Huber ministat). The outlet was connected to a diaphragm vacuum pump (vacuubrand, ME 2C, 1.9/2.2m³/h, 80 mbar). The device was placed on a microscope, in an incubating chamber (30°C). Once the pump was turned on, PBS washed through the tubing into the main flow channel and entered by capillary into the compartments within a couple of minutes. Air was pushed outside through the PDMS. The experiment began by replacing the PBS with cell extract, which then washed through the main flow channel at a rate of ~1 μ l/min and diffused through the capillaries into DNA compartments. Constant flow was maintained during the experiment.

Imaging

The experiment was carried on a translational stage coupled to an inverted microscope (Zeiss Axiovert 200) with ANDOR Neo sCMOS camera (Andor Technology plc., Belfast, UK) and X10 Zeiss objective.

DNA Brush

Using our photolithography approach DNA-SA conjugates assembled on a pre-patterned biotin surface. The DNA bound to the surface at high densities to form DNA brushes which we have extensively studied in previous publications (16, 17). The assembly protocol is described in detail in the previous section, and here we review some of the brush characteristics.

Brush properties

The DNA brush is a dense phase of DNA molecules that are anchored to the surface at one end. The density of surface binding sites is estimated $10^4 \mu\text{m}^{-2}$ and the final DNA brush density is at the order of $10^3 \mu\text{m}^{-2}$ such that the distance between DNA molecules is $\sim 20 \text{ nm}$. At such proximity the charged DNA polymers experience electrostatic and excluded volume interactions, that can stretch the brush perpendicular to the surface (24). In water, the brush is fully extended to its contour length, due to osmotic pressure of counter ions that are trapped within the brush to maintain neutrality. In a buffered solution with ionic strength of $\sim 150 \text{ mM}$, electrostatic interactions are screened out and a 1 kbp DNA brush attains a minimal height of $\sim 100 \text{ nm}$. Thus, the effective DNA concentration in the brush is $\sim 10 \mu\text{M}$ which is 3 orders of magnitude higher than the concentration that is typically used in cell-free reactions (bulk or vesicle) (2, 19).

Promoter orientation

In the linear DNA constructs used in this work, the promoter was oriented towards the surface of the compartment. The gene size varied 300-1000bp. The distance between the DNA top and the promoter is about 200bp and a similar distance between the terminator and the DNA end attached to the surface. We have studied the effect of promoter orientation and surface proximity on transcription activity in a previous publication (5). There, we observed that transcription activity is enhanced when the promoter is pointing towards the surface and located close to the surface (25).

The endogenous E. Coli cell-free extract

Overview

In this study we used a cell-extract that is a crude cytoplasmic extract from *E. Coli* strain BL21 Rosetta2 (Novagen) according to a procedure described previously (18). The cell-free reactions were composed of 33% (volume) crude extract and the other 66% (volume) of water, DNA and buffer with the following final composition: 50 mM HEPES pH 8, 1.5 mM ATP, 1.5 mM GTP, 0.9 mM CTP, 0.9 mM UTP, 0.2 mg/mL tRNA, 0.26 mM coenzyme A, 0.33 mM NAD, 0.75 mM cAMP, 0.068 mM folinic acid, 1 mM spermidine,

30 mM 3-phosphoglyceric acid, 2 mM DTT, 1.5 mM amino acids, 6.5 mM Mg-glutamate, 100 mM K-glutamate, and 2% PEG 8000.

Here we briefly review the cell-extract with a focus on the transcription/translation machinery, nucleases and proteases.

Enzymes in the cell-extract

The extract contained the soluble proteins of *E. coli* (above 10 kDa molecular weight cut-off), with concentrations of 10 mg/ml in the final reaction, which was the optimum concentration for expression (18). The liquid part of the cell (cytoplasm) was extracted by breaking the cells. Membranes and insoluble debris were removed by centrifugation. During extract preparation, the endogenous DNA and mRNA were removed. The cell extract provided the transcription and the translation machineries necessary for gene expression. The transcription was driven by the endogenous *E. coli* RNA polymerase and thus allowed us to use the entire repertoire of the *E. Coli* regulation toolbox (19). This was the major difference with standard extracts, which use bacteriophage RNA polymerases.

Nuclease and protease activity

The cell extract contained active proteases and ribonucleases. Previously, we studied the stability of proteins and mRNA in our cell-free system (21, 26). Proteins without a degradation tag were stable with no observed degradation. Proteins with degradation tags, such as SsrA and YbaQ, were targeted to the ClpXp degradation complex and were degraded with a fast initial degradation rate of 10nM/min but the degradation activity was lost after a degradation of $\sim 0.5\mu\text{M}$ in the cell extract. In contrast, mRNA exhibited a lifetime of about 10 minutes and was degraded by non-specific ribonucleases. The protein GamS, was added to all of the reactions in concentration of $3\mu\text{M}$ to inhibit the degradation of linear DNA by the 3' exonuclease activity of the RecBCD complex (27) which was present in the cell-free system.

Energy regeneration system

The cell-extract was supplemented with 3-phosphoglyceric acid (3-PGA) for ATP regeneration (18). The 3-PGA is a natural substrate to *E. Coli* and therefore no enzyme was added to the extract.

Arabinose Supplement

In experiments including the positive feedback construct, with the AraC promoter, we added 1.5% (W/V) final concentration of arabinose (A3256 - L-(+)-Arabinose, Sigma).

Calibration of GFP concentration and diffusion

GFP concentration

In order to assess the GFP concentration expressed in the microfluidic chamber we performed a calibration measurement. Recombinant purified GFP at different concentrations was continuously flown through the main channel and diffused into the

capillaries and finally into the compartment. We measured the fluorescence in the compartment as a function of GFP concentration (Fig. S4).

GFP diffusion coefficient

We evaluated GFP diffusion coefficient by pumping 1 μ M of GFP through the main flow channel. GFP diffused through the capillary channels and into the chambers (Fig. S4). The diffusion coefficient D was calculated,

$$D = \frac{L^2}{T_{GFP}} = 33.5 \pm 1 \frac{\mu m^2}{s}.$$

Here T_{GFP} was the diffusion time of GFP, L was the length of the capillary channel.

Expression dynamics Variation

We studied variation of expression dynamics between compartments within a single experiment, and between different experiments using the unregulated construct expressing GFP under a P_{70} promoter (Fig. S9) and for the self-repressing construct (Fig. S10). We estimated the variation as the standard deviation of the relative difference between two compartments.

$$\% \text{ variation} = 100 \cdot \text{std} \left(\frac{\sqrt{(P_1 - P_2)^2}}{P_1} \right)$$

Here P_1, P_2 is GFP expression level in compartments 1 and 2 with the same characteristic geometrical parameters, and the standard deviation was taken over all time points in the same experiment. The variation between different experiments is 5-10%. The variation between compartments in the same experiment is less than 3%.

Protease activity in the DNA compartment

In principle, adding protein degradation tags may further shorten the lifetime of proteins in the compartment, leading to shorter time scales in the dynamics. However, targeting degradation of GFP fused to SsrA or YbaQ tags by the ClpXP complex endogenously present in the cell-free extract (21) showed no detectable difference in kinetics (Fig. S13).

Supplementary Text

Single compartment Theory: the effective lifetime

The dynamics of proteins in the device is decoupled into (i) synthesis inside the compartment with a diffusive leak into the capillary, and (ii) one-dimensional diffusion along the capillary,

$$\dot{p} = D\nabla^2 p.$$

Here D is the protein diffusion coefficient. We will assume an adiabatic approximation such that the diffusion dynamics along the capillary is slower than the protein dynamics in the compartment and therefore can be assumed at steady state,

$$\begin{aligned} p(x, t) &= p_R(t)(1 - x/L), \\ \partial_x p(x, t) &= -p_R(t)/L. \end{aligned}$$

Here p_R is the protein concentration in the compartment, where it is homogenous. There is a linear concentration profile along the capillary of length L , which reaches zero at the main channel, $x = L$ (Fig. S5). The time scale for reaching linear gradient is $\tau_D = L^2/D \approx 5 \text{ min}$.

The diffusion of proteins from the compartment into the capillary can be computed by writing the diffusion equation inside the two-dimensional compartment.

$$\partial_t p_R(r, t) = D\nabla^2 p_R(r, t) + a_{syn}.$$

The first term is the diffusion within the compartment and the second term is the protein synthesis rate per unit volume. We integrate this equation up to the compartment boundary $r = R$ using gauss's law, $\int dV \nabla^2 p = \int ds \hat{n} \cdot \bar{\nabla} p$,

$$\partial_t p_R(t) = a_{syn} + \frac{D}{V} \int ds \hat{n} \cdot \bar{\nabla} p_R(R, t).$$

Here $V = \pi R^2 h$ is the compartment volume. The boundary condition along the compartment walls is $\nabla p_R(R, t) = 0$, except for the compartment opening. The opening has width W and height h , and the protein gradient is along the capillary, $\int ds \hat{n} \cdot \bar{\nabla} p_R(R, t) = hW \partial_x p_R$. We thus obtain,

$$\partial_t p(t) = a_{syn} + \frac{DhW}{V} \partial_x p_R.$$

The gradient at the compartment opening is $\partial_x p_R = -p_R/L$ and thus,

$$\partial_t p(t) = a_{syn} - \frac{DW}{\pi R^2 L} p_R.$$

We define the effective protein lifetime,

$$\tau_R = \frac{V_R}{V_c} \tau_D = \frac{\pi R^2}{DW} L$$

and the protein dynamics inside the compartment is,

$$\partial_t p_R = a_{syn} - p_R/\tau_R.$$

For diffusion coefficient, $D = 33\mu m^2/s$, and for the $300\mu m$ long capillary, the protein life time is $\tau_R = 60 min$.

The steady state solution in the compartment is,

$$p_R = a_{syn} \tau_R = a_{syn} \frac{\pi R^2 L}{DW}.$$

The gradient slope is independent of the capillary length,

$$\partial_x p = -\frac{a_{syn} \tau_R}{L} = a_{syn} \frac{\pi R^2}{DW}.$$

Single compartment theory: Gene expression onset time

In this section we derive an equation for the onset time of expression in the DNA compartments. We find that the onset time scales linearly with the capillary length, $t_{onset} \sim L$, as observed experimentally (Fig. S7).

The expression initiates once a minimal concentration c_{onset} of the reaction components reaches the compartment. The diffusion of reaction components can be divided in two steps: i) Fast diffusion, $\tau_D = L^2/D$, along the one-dimensional capillary. ii) A slower regime determined by a time scale, τ_R , which is similar to the protein lifetime described in the previous section. In this regime, the reaction components reach the two-dimensional compartment, and a linear concentration gradient forms between the flow channel where the concentration is maximal c_{max} to the compartment where the concentration $c(t)$ is initially zero, $c(0) = 0$, and increases with time to $c = c_{max}$. Using Fick's law the flux of reaction components into the DNA compartment is,

$$J \left[\frac{mol}{m^2s} \right] = -D \frac{\partial c}{\partial x}.$$

Assuming a linear gradient between the compartment and the flow channel we find the kinetics of reaction components inside the compartment,

$$\dot{c} = -\frac{c_{max}-c}{\tau},$$

$$c = c_{max} \left(1 - e^{-\frac{t}{\tau}} \right),$$

$$\tau = \frac{\pi R^2 L}{DW}.$$

We further assume that the minimal concentration for expression onset c_{min} is smaller than the final concentration $c_{onset} < c_{max}$. We derive the onset time,

$$c_{onset} = c_{max} \left(1 - e^{-\frac{t_{onset}}{\tau}} \right),$$

$$t_{onset} \approx \frac{c_{min}}{c_{max}} \tau \sim L.$$

Indeed, we find that the expected onset time is linear in the capillary length.

One-dimensional array of connected compartments: Expression and diffusion

We consider a one-dimensional array of connected compartments (Fig. 4). In this case, proteins are synthesized in a single compartment and diffuse between compartments (x-axis) along capillaries with width W_x and length L_x (Fig. S16). In addition, the proteins diffuse in the y-axis out to the main channel, along capillaries with width W_y and length L_y , which is the turnover mechanism described in the previous section. At steady state we expect the concentration within the compartments to be homogenous, and to have linear profiles along the capillaries and between compartments. The linear profiles are the steady-state solution to the one-dimensional diffusion equation along the capillaries.

In this section we use the above considerations to show that the steady-state profile of proteins along the one-dimensional array of compartments is exponentially decaying away from the protein source. The decaying profile has an exponential envelope, which is composed of small linear decays between compartments. Thus, at the length scale of a single compartment, we observe a linear decay. At larger scales, the observed decay is exponential. We find that the exponential decay length, $\lambda = \sqrt{D_{eff} \tau}$, can be expressed in terms of an effective diffusion coefficient, D_{eff} , and the lifetime of proteins in the compartment, τ .

Notably, the decay length scales with the compartment geometry but is independent of the protein diffusion coefficient. This is because both the effective diffusion coefficient as well as the protein lifetime, result from the protein diffusion.

The flux of proteins from the compartment into the capillaries is,

$$J \left[\frac{mol}{m^2 s} \right] = -D \frac{\partial p}{\partial x}$$

Assuming linear profiles along the capillaries, the flux of proteins into the capillaries in units of concentration per unit time is,

$$\dot{p} = -\frac{DW}{\pi R^2 L} \Delta p = -\frac{\Delta p}{\tau}$$

We define two time scales for the diffusion along the x-axis,

$$\tau_x = \frac{\pi R^2 L_x}{DW_x}$$

and for the diffusion along the y-axis,

$$\tau_y = \frac{\pi R^2 L_y}{DW_y}$$

We consider the protein kinetics in compartment i . The proteins can diffuse to compartment $i - 1$, to compartment, $i + 1$, or to be depleted into the main channel. The kinetic equation is,

$$\dot{p}_i = 1/\tau_x (p_{i-1} - p_i) + 1/\tau_x (p_{i+1} - p_i) - p_i/\tau_y$$

We obtained a discrete one-dimensional diffusion equation with effective diffusion constant $D_{Eff} = d^2/\tau_x$ and protein lifetime τ_y . The distance between compartments is $d = R + L_x$.

$$\dot{p}_i = D \frac{p_{i-1} + p_{i+1} - 2p_i}{d^2} - \frac{p_i}{\tau_y}$$

The steady-state solution is an exponential decay,

$$p_i = p_1 e^{-(i-1) \cdot \frac{d}{\lambda}}$$

The exponential decay length is,

$$\lambda = \frac{d}{\cosh^{-1}\left(\frac{d^2}{2D\tau_y} + 1\right)}$$

The decay length is simplified in the limit where it is larger than the distance between compartments $d < \sqrt{D\tau_y}$ (the continuum limit),

$$\lambda \approx \sqrt{D\tau_y} = d \sqrt{\frac{L_y W_x}{L_x W_y}},$$

The decay length scales with the distance between compartments and the square root of the ratio between geometrical parameters of the capillaries. Interestingly, the decay length is independent of the diffusion coefficient of the protein. Thus the same decaying length is expected for different proteins. In the experiment (Fig. 4) we find that the GFP profile along the x – axis has an envelope of an exponentially decaying profile, with a decay length of $\lambda = 380 \pm 40\mu m$, while the exponential profile expected for this one-dimensional expression diffusion system with $L_x = 100\mu m; W_x = 20\mu m; L_y = 150\mu m; W_y = 20\mu m$, is $\lambda = 280\mu m$. The difference between the estimated theoretical value and the measured value of the decay length is reasonable given the array is composed only of 7 reactors whereas the theory considers an infinite array.

One-dimensional array of connected compartments: Flow considerations

The flow in the microfluidic device is laminar. The capillary connecting the compartments is parallel to the main channel, and there is a pressure gradient between the first and last compartments. Thus, we expect a residual flow between compartments (Fig. S16). Here we show that our design minimizes the flow between the compartments and that the dominant transport between compartments is by diffusion.

The flow rate through the device in the 1D experiments was $Q \approx 0.3\mu l/min$. The feeding channel was $900\mu m$ wide and $100\mu m$ deep with a cross section area $A_{main} \approx 10^5\mu m^2$. Thus the velocity in the feeding channel was $v_{main} = Q/A \approx 50\mu m/s$. The hydraulic resistance determines the ratio of velocities between the main channel and the capillary,

$$\frac{v_{cappillary}}{v_{main}} = \frac{R_{main} A_{main}}{R_{capillary} A_{capillary}} = \left(\frac{h_{capillary}}{h_{main}} \right)^2 \approx 10^{-4}.$$

Here we used the Poiseuille equation for hydrodynamic resistance in a rectangular cross section, $R = \frac{12\eta L}{h^3 W}$. The liquid viscosity is η . Thus, the velocity in the capillary connecting the compartments is $v_{capillary} = 5 \cdot 10^{-3}\mu m/s$.

We compare the transport distance by flow and diffusion during the lifetime of proteins in the compartments, $\tau \approx 60 min$ which was derived in previous sections:

$$\begin{aligned} L_{flow} &= v_{cappillary}\tau \approx 15\mu m, \\ L_{Diffusion} &= \sqrt{D_{eff}\tau} \approx 350\mu m. \end{aligned}$$

Indeed we see that during the lifetime of proteins in the compartments, their transport by diffusion is dominant over the transport by flow, $L_{Diffusion} \gg L_{flow}$.

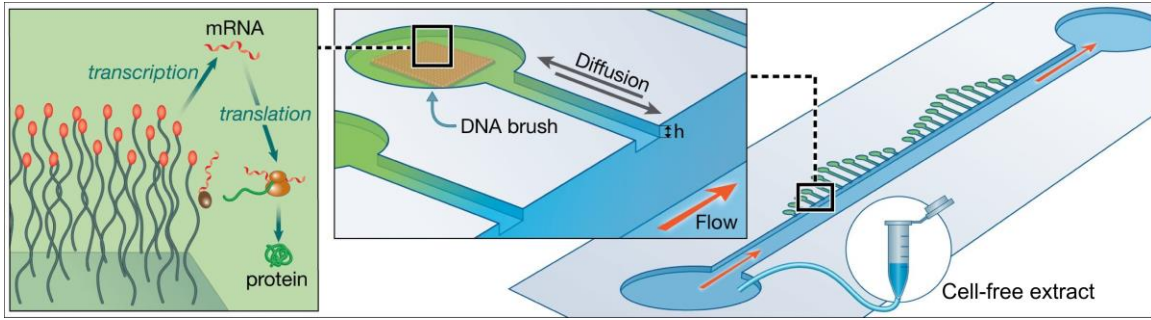


Fig. S1. Microfluidic device and the DNA compartment

DNA brushes patterned (red squares) in circular compartments carved in silicon and connected to a flow channel through a diffusive capillary. The transcription/translation cell extract enters into the thin capillaries ($h = 1 - 3\mu m$) from the main flow channel ($h = 30\mu m$) only by diffusion. Proteins expressed from the brush diffuse to the flow channel setting up a source-sink linear gradient.

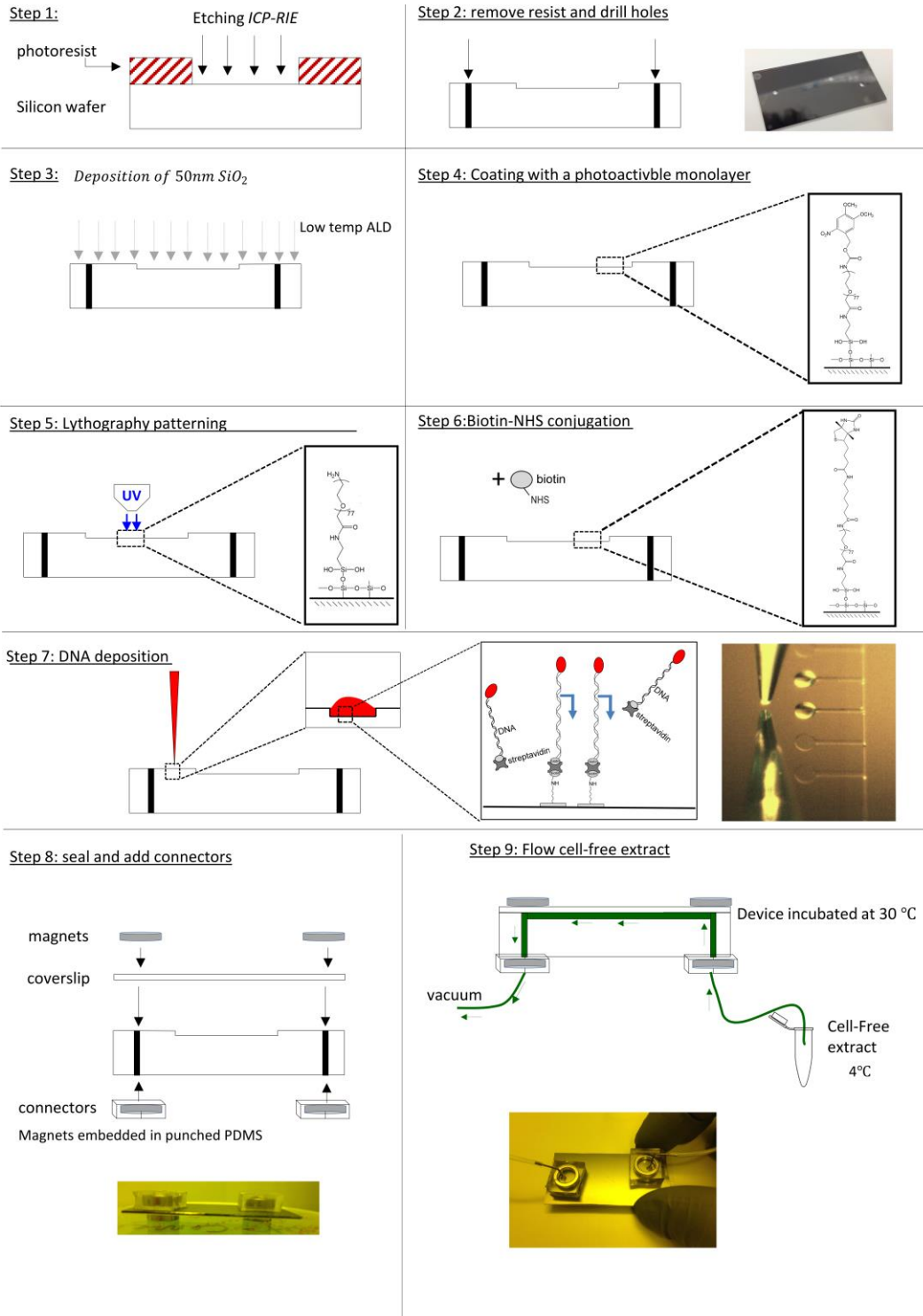


Fig. S2. Fabrication and assembly of the microfluidic device
Steps are detailed in the text.

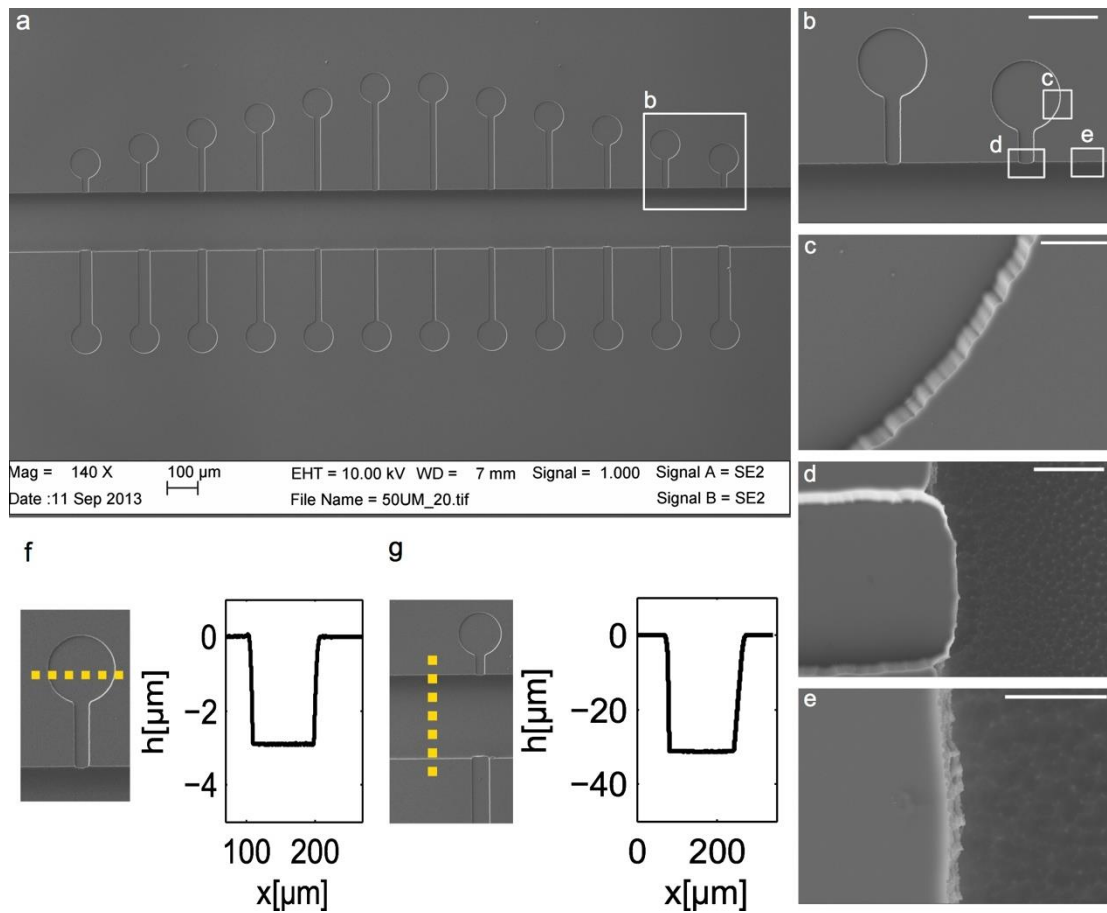


Fig. S3. SEM measurement of the silicon device.

(a) Reactor etched deep connected to a deep flow channel. (b) Magnification of two reactors. Scale bar μm . (c) Magnification of the chamber wall. Scale bar μm . (d) Magnification of the interface between the capillary channel and the flow channel. Scale bar is $5\mu\text{m}$. (e) Magnification of the main channel wall. Scale bar $2\mu\text{m}$. (f) Height profile measurement of the compartment (along dashed yellow line). (g) Height profile measurement of the main channel (along dashed yellow line).

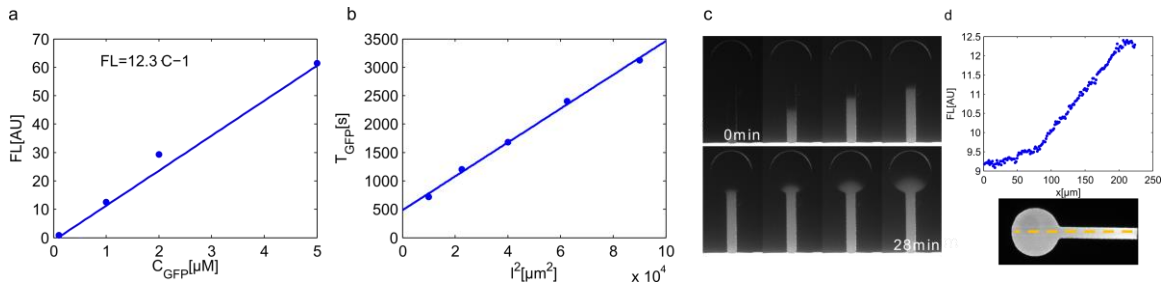


Fig. S4. GFP calibration and diffusion into the compartments

(a) Calibration of the concentration of GFP expressed in the microfluidic chamber. Fluorescent intensity measurements versus protein concentrations. (b) Measurement of GFP diffusion time along the capillary from the flow channel up to the chamber as a function of capillary channel length. (c) Fluorescence time-lapse images of GFP diffusing along the $200 \mu\text{m}$ capillary from the flow channel into the chamber. Scale bar $100 \mu\text{m}$. (d) GFP profile between the main channel and the DNA-compartment. The main channel was first filled with PBS and then with GFP. GFP formed a linear concentration gradient from a maximal value in main channel down to the compartment.

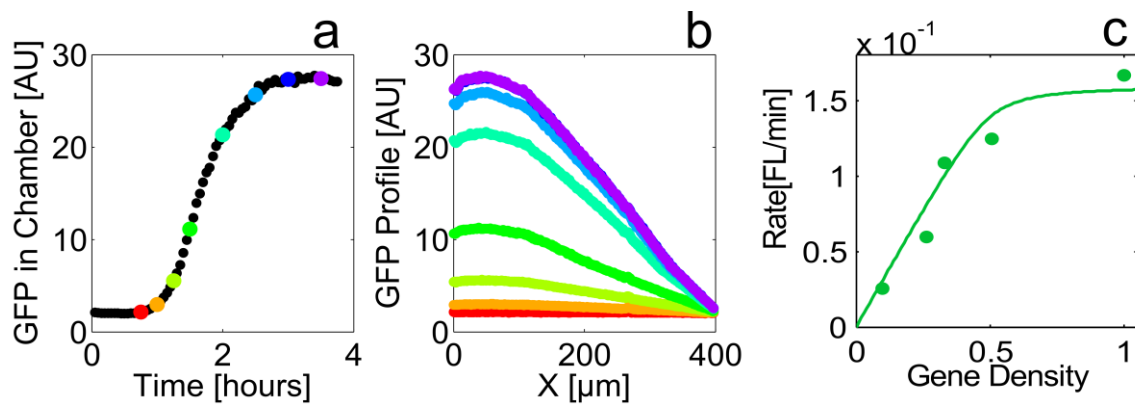


Fig. S5. Kinetics and linear profile of GFP

(a) GFP intensity in arbitrary units (AU) in the DNA compartment as a function of time, for $L = 300\mu m$. (b) GFP profile along the capillary at different time points indicated by color code matching the colored time points in (a). (c) GFP expression rate at the first hour of expression ($L = 300\mu m$) as a function of the gene density given in ratio of GFP coding DNA to non-coding DNA.

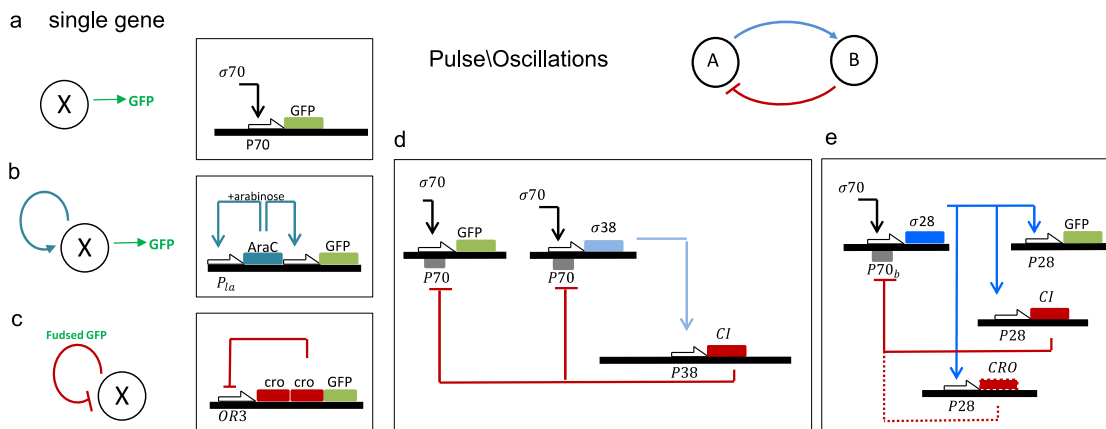


Fig. S6. Activator and repressor network scheme.

(a) Unregulated gene activated from σ^{70} factor in the extract solution and expressing GFP. (b) A construct with positive feedback expressing *araC* activator and GFP. (c) A construct with negative feedback expressing GFP fused to a Cro repressor dimer. (d) An activator repressor network with activator σ^{38} and repressor *cI*. (e) An activator repressor network with activator σ^{28} with repressors *cI* and Cro.

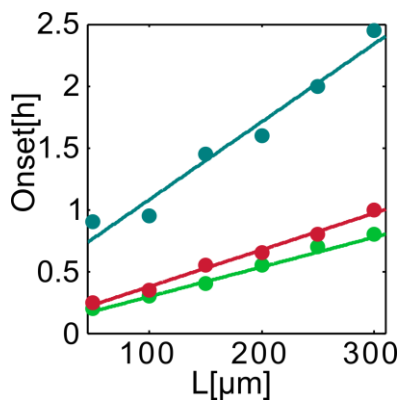


Fig. S7. GFP Expression Onset time.

Onset time of GFP in the chamber as a function of the capillary length for the different constructs: unregulated (green dots), positive feedback (blue dots) and negative feedback (red dots).

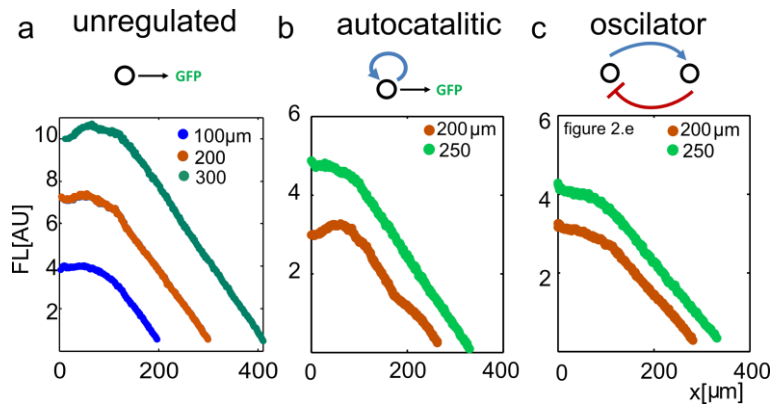


Fig. S8. GFP profile slope

GFP profile along the capillary in (a) unregulated construct for lengths $100 \mu\text{m}$, $200 \mu\text{m}$, and $300 \mu\text{m}$. (b) Autocatalytic construct for lengths $200 \mu\text{m}$ and $250 \mu\text{m}$. (c) Oscillator construct for lengths $200 \mu\text{m}$ and $250 \mu\text{m}$. Gradient slope is independent of capillary length.

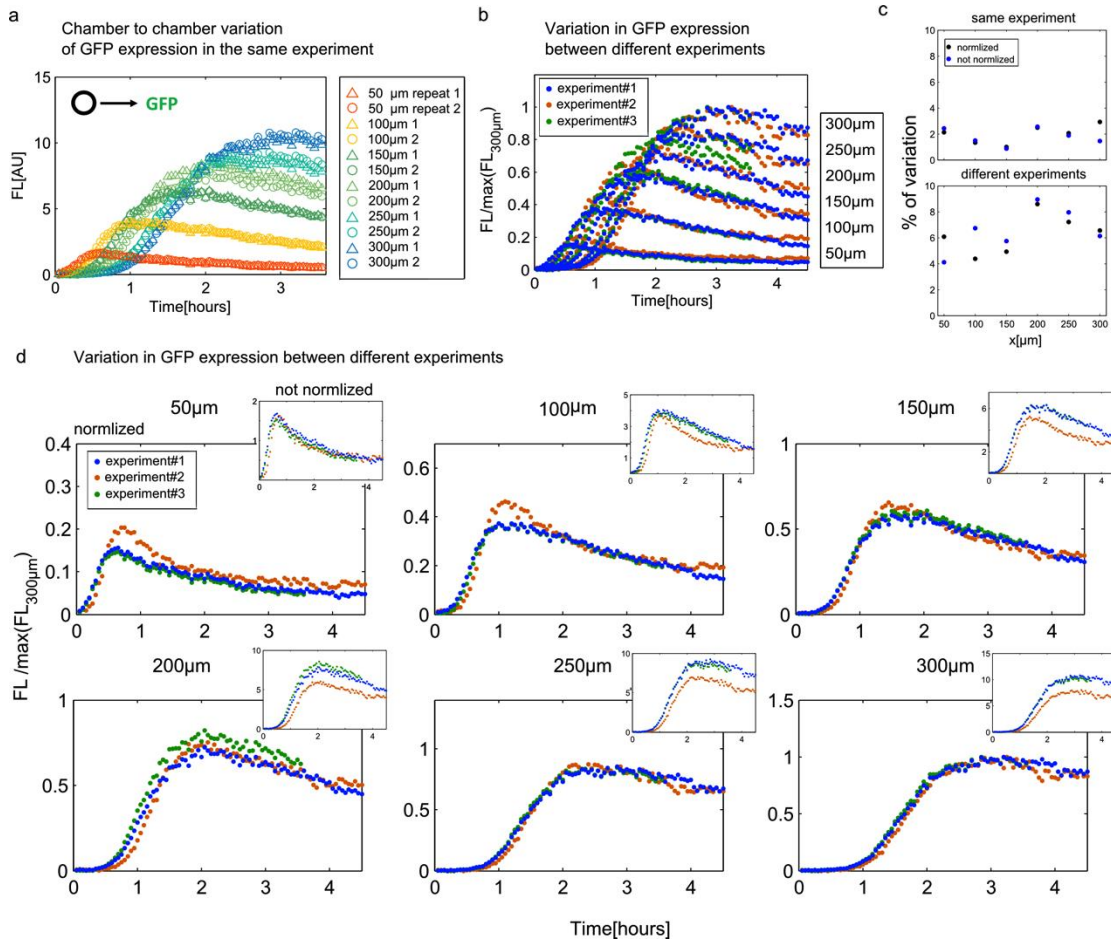


Fig. S9. Gene expression variation for the unregulated construct.

(a) Variation of GFP expression between compartments in the same experiment for the unregulated construct. Two repeats of expression kinetics in the DNA compartment for varying capillary length $L = 50 - 300 \mu\text{m}$. (b) Variation of GFP expression between compartments in three different experiments for varying capillary length. GFP expression is normalized to the maximal intensity value of the capillary $L = 300 \mu\text{m}$ within a single experiment. (c) Percentage of chamber to chamber variation in the same experiment, and between different experiments as a function of capillary length for normalized and non-normalized kinetics. The variation is calculated as the standard deviation of the relative difference between two identical compartments. (d) Normalized GFP dynamics in the DNA chamber for three experiments, and (inset) non-normalized dynamics.

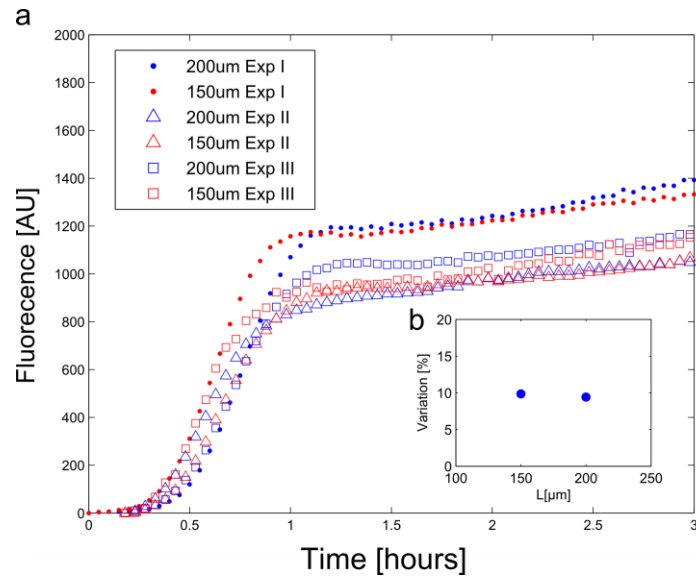


Fig. S10. Gene expression variation for the self-repressing construct.

(a) Variation of expression between compartments in different experiments for a construct with negative feedback expressing GFP fused to a Cro repressor dimer. Three repeats of expression kinetics in the DNA compartment for two capillary lengths μm . (b) Percentage of chamber to chamber variation as a function of capillary length.

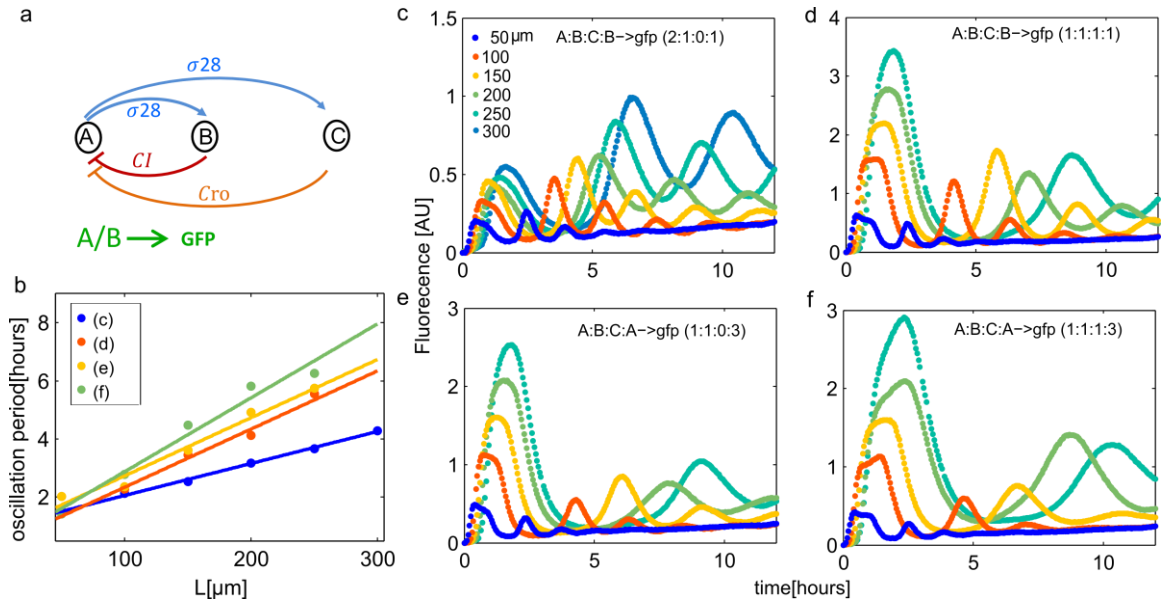


Fig. S11. Oscillatory networks

(a) Network scheme. Activator is the sigma factor, σ^{28} , coded by gene A. Two repressor proteins were lambda phage CI (coded by gene B) and Cro (coded by gene C). The four networks are detailed in Table S3. (b) Oscillation period as a function of capillary length for the four networks (c-f). (c-f) GFP kinetics as a function of time. Networks numbers are: (c) 2, (d) 3, (e) 4, (f) 5 as detailed in Table S3.

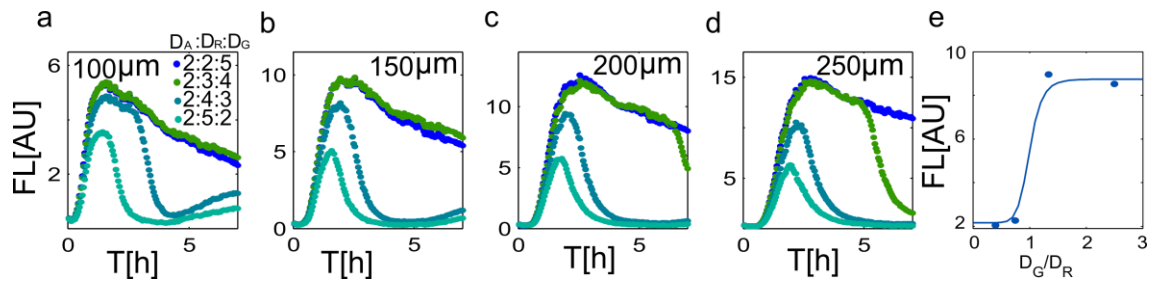


Fig. S12. Activator and repressor pulse dynamics.

(a-d) GFP dynamics of the $\sigma^{38} - cl$ activator-repressor network at different Activator : Repressor : GFP reporter DNA ratios ($D_A:D_R:D_G$) and at varying capillary length μm . The GFP reporter is under the activator promoter. (e) GFP levels as a function of DNA stoichiometry D_G/D_R after 5 hours of expression for $L = 200\mu m$. Network is detailed in Table S3.

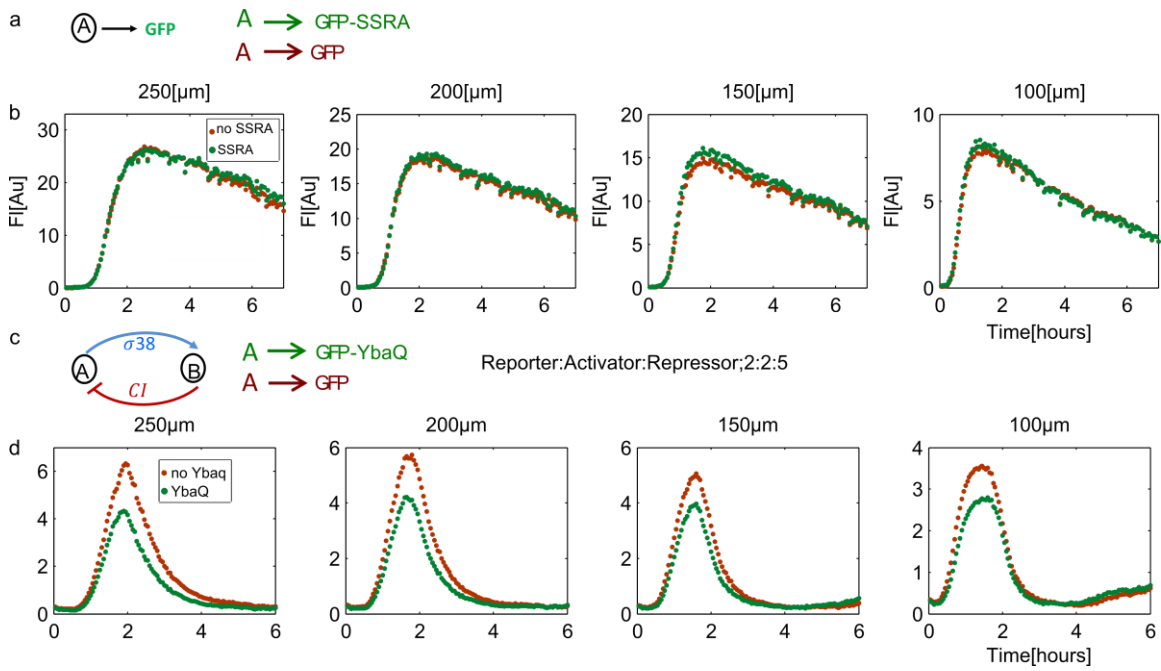


Fig. S13. Protein degradation by ClpXp

(a-b) Dynamics of GFP expression with GFP fused to SsrA degradation tag in an unregulated construct for capillary lengths $L = 100 - 250 \mu m$. (c-d) Dynamics of GFP expression with GFP fused to YbaQ degradation tag in an activator repressor network ($\sigma^{38} - CI$, Network 1) for capillary lengths $L = 100 - 250 \mu m$.

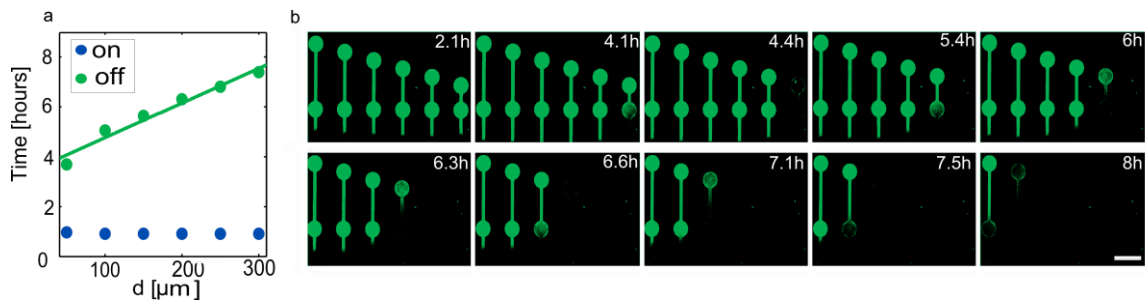


Fig. S14. Communication between connected DNA compartments

(a) Expression onset (blue) and offset (green) times as a function of distance between the two compartments, as determined by measuring the time of GFP levels above 100 [AU] and below $2.5 \cdot 10^3$ [AU], respectively. The solid line is a linear fit. (b) GFP time lapse images, showing hierarchal shut down with distance between the two compartments. To improve contrast the image maximal intensity was set at $5 \cdot 10^3$ [AU]. Scale bar $200\mu\text{m}$.

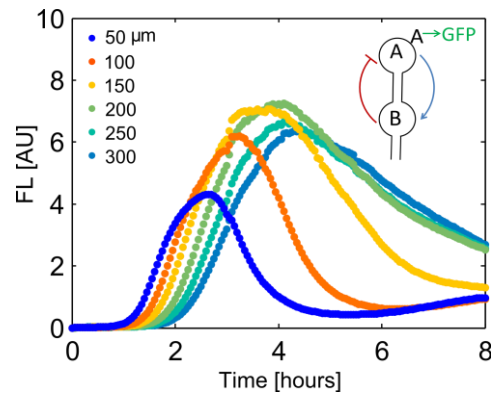


Fig. S15. Communication between connected DNA compartments for genes patterned in reverse order.

GFP kinetics as a function of time for an activator-repressor network patterned in two connected compartments. Compartment B is $100\mu m$ away from the flow channel and patterned with the CI repressor genes. Compartment A is located at a distance d from compartment B, and contains σ^{38} activator and GFP reporter genes (network 1).

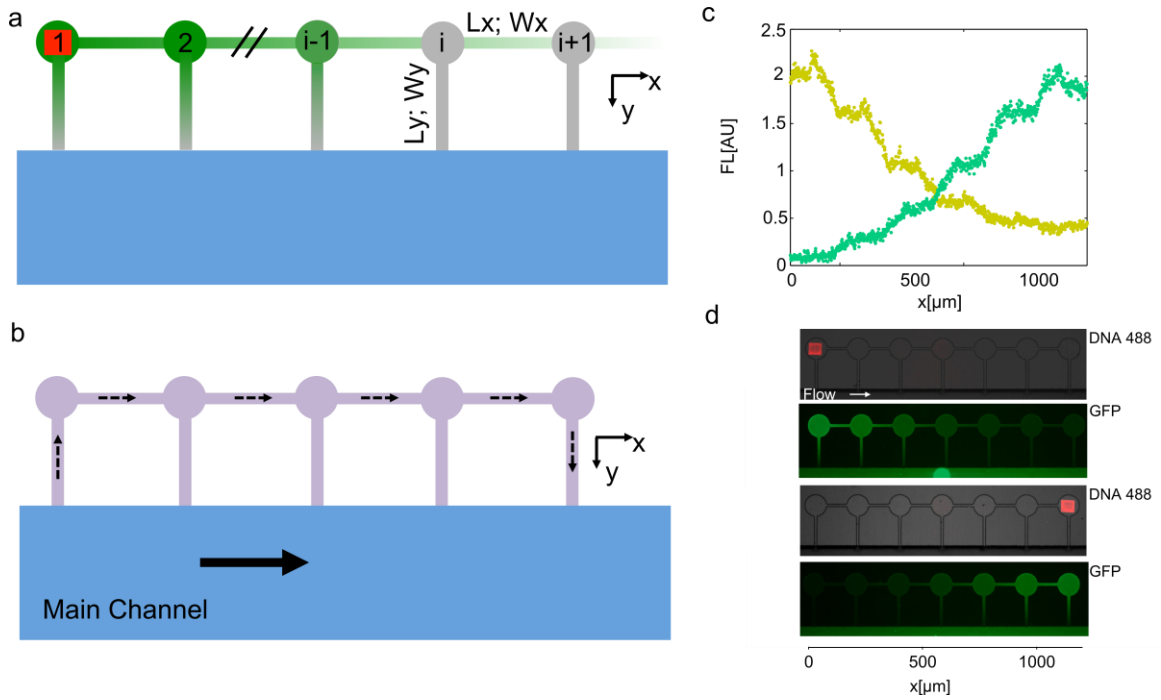


Fig. S16. One-dimensional array of connected compartments.

(a) Illustration of an array of connected compartments. DNA source is in chamber number 1 and the synthesized protein diffuses to the adjacent compartments along the x-axis. In addition, the protein diffuses along the y-axis to the main channel and evacuates from the chambers. (b) Flow profile along the capillaries and in the main channel. Our design minimized the flow between the compartments. (c) GFP expression profile along the x-axis generated from a source that is located along (yellow) and against (green) the direction of flow. The GFP intensity is homogenous within a compartment, decays linearly between two neighboring compartments. (d) Fluorescent images of DNA brushes (red label, 647nm) before expression and the GFP images along and against the direction of flow.

Promoter	Description	Reference
P ₇₀	Lambda phage promoter OR2-OR1-Pr specific to E. coli σ^{70} . Repressed by cI at high affinity and Cro with low affinity.	(18)
P _{70b}	Promoter of the Lambda Cro repressor with the operator OR3 specific to E. coli σ^{70} . Repressed by Cro.	This work
P ₂₈	Promoter of the tar gene (E. coli) specific to σ^{28}	(19)
P ₃₈	Promoter of the osmY gene (E. coli) specific to σ^{38}	(19)
Plac\arac (<i>P_{la}</i>)	The hybrid promoter pLacO-1	(20)
Untranslated region		
UTR1	The untranslated region containing the T7 g10 leader sequence for highly efficient translation initiation	(19)
Transcription terminator		
T500	Transcription terminator for E. coli RNA polymerase	(19)
Gene		
GFP	The enhanced green fluorescent protein truncated and modified in N- and C- termini.	(19)
σ^{28}	rpoF (E. coli σ^{28})	(19)
σ^{38}	rpoS (E. coli σ^{38})	(19)
CI	Lambda phage repressor protein CI	(19)
CRO	Lambda phage repressor protein Cro	(19)
diCro-GFP	Triple fusion protein Cro-Cro-GFP	This work
araC	AraC protein with ssra degradation tag	(20)
yemGFP	Monomeric yeast-enhanced green fluorescent protein with ssrA degradation tag	(20)

Table S1. DNA Modules

Construct	Description	Figure
unregulated		Fig 1c, Fig 2a, Fig 4a-c, Fig S5, Fig S8a, Fig S9, Fig S13a Fig S16c-d
positive feedback		Fig 1d, Fig 2b, Fig S8b
negative feedback		Fig 1f, Fig 2c, Fig S10

Table S2. DNA Constructs – Single Gene

	Description	DNA Stoichiometry	
Network 1	Appearing in	Fig 2e, Sig S12	Fig S6
	Activator	2	Color coded in Figure
	Repressor	2	
	Reporter	5	
Network 2	Appearing in	Fig 1e, Fig 2d, Fig S11b	
	Activator	2	
	Repressor	1	
	Reporter	2	
Network 3	Appearing in	Fig S11c	
	Activator	1	
	Repressor	1	
	Reporter	3	
Network 4	Appearing in	Fig S8c, Fig S11d	
	Activator	1	
	Repressor1	1	
	Repressor 2	1	
	Reporter	1	
Network 5	Appearing in	Fig S11e	
	Activator	1	
	Repressor1	1	
	Repressor 2	1	
	Reporter	3	

Table S3. DNA Constructs – Activator-Repressor networks

Movie S1

Fluorescence time-lapse images showing onset of GFP expression in the compartments for the unregulated construct. Film duration 4.5h (Film showing 3 frames / sec, images were taken every 3 minutes in the experiment).

Movie S2

Fluorescence time-lapse images showing GFP expression dynamics in an activator-repressor network implemented into two connected chambers. Film duration 3.9h (Film showing 6 frames / sec, images were taken every 3 minutes in the experiment).

References and Notes

1. D. S. Tawfik, A. D. Griffiths, Man-made cell-like compartments for molecular evolution. *Nat. Biotechnol.* **16**, 652–656 (1998). [Medline doi:10.1038/nbt0798-652](#)
2. V. Noireaux, A. Libchaber, A vesicle bioreactor as a step toward an artificial cell assembly. *Proc. Natl. Acad. Sci. U.S.A.* **101**, 17669–17674 (2004). [Medline doi:10.1073/pnas.0408236101](#)
3. V. Noireaux, R. Bar-Ziv, A. Libchaber, Principles of cell-free genetic circuit assembly. *Proc. Natl. Acad. Sci. U.S.A.* **100**, 12672–12677 (2003). [Medline doi:10.1073/pnas.2135496100](#)
4. J. Kim, K. S. White, E. Winfree, Construction of an in vitro bistable circuit from synthetic transcriptional switches. *Mol. Syst. Biol.* **2**, 68 (2006). [Medline doi:10.1038/msb4100099](#)
5. E. Franco, E. Friedrichs, J. Kim, R. Jungmann, R. Murray, E. Winfree, F. C. Simmel, Timing molecular motion and production with a synthetic transcriptional clock. *Proc. Natl. Acad. Sci. U.S.A.* **108**, E784–E793 (2011). [Medline doi:10.1073/pnas.1100060108](#)
6. A. J. Hockenberry, M. C. Jewett, Synthetic in vitro circuits. *Curr. Opin. Chem. Biol.* **16**, 253–259 (2012). [Medline doi:10.1016/j.cbpa.2012.05.179](#)
7. M. Isalan, C. Lemerle, L. Serrano, Engineering gene networks to emulate *Drosophila* embryonic pattern formation. *PLoS Biol.* **3**, e64 (2005). [Medline doi:10.1371/journal.pbio.0030064](#)
8. D. Matthies, S. Haberstock, F. Joos, V. Dötsch, J. Vonck, F. Bernhard, T. Meier, Cell-free expression and assembly of ATP synthase. *J. Mol. Biol.* **413**, 593–603 (2011). [Medline doi:10.1016/j.jmb.2011.08.055](#)
9. Y. Heyman, A. Buxboim, S. G. Wolf, S. S. Daube, R. H. Bar-Ziv, Cell-free protein synthesis and assembly on a biochip. *Nat. Nanotechnol.* **7**, 374–378 (2012). [Medline doi:10.1038/nnano.2012.65](#)
10. J. Shin, P. Jardine, V. Noireaux, Genome replication, synthesis, and assembly of the bacteriophage T7 in a single cell-free reaction. *ACS Synth. Biol.* **1**, 408–413 (2012). [Medline doi:10.1021/sb300049p](#)
11. A. S. Spirin, V. I. Baranov, L. A. Ryabova, S. Y. Ovodov, Y. B. Alakhov, A continuous cell-free translation system capable of producing polypeptides in high yield. *Science* **242**, 1162–1164 (1988). [Medline doi:10.1126/science.3055301](#)
12. T. Thorsen, S. J. Maerkl, S. R. Quake, Microfluidic large-scale integration. *Science* **298**, 580–584 (2002). [Medline doi:10.1126/science.1076996](#)
13. D. Gerber, S. J. Maerkl, S. R. Quake, An in vitro microfluidic approach to generating protein-interaction networks. *Nat. Methods* **6**, 71–74 (2009). [Medline doi:10.1038/nmeth.1289](#)
14. H. Niederholtmeyer, V. Stepanova, S. J. Maerkl, Implementation of cell-free biological networks at steady state. *Proc. Natl. Acad. Sci. U.S.A.* **110**, 15985–15990 (2013). [Medline doi:10.1073/pnas.1311166110](#)
15. P. Müller, K. W. Rogers, S. R. Yu, M. Brand, A. F. Schier, Morphogen transport. *Development* **140**, 1621–1638 (2013). [Medline doi:10.1242/dev.083519](#)

16. A. Buxboim, M. Bar-Dagan, V. Frydman, D. Zbaida, M. Morpurgo, R. Bar-Ziv, A single-step photolithographic interface for cell-free gene expression and active biochips. *Small* **3**, 500–510 (2007). [Medline doi:10.1002/sml.200600489](#)
17. D. Bracha, E. Karzbrun, S. S. Daube, R. H. Bar-Ziv, Emergent properties of dense DNA phases toward artificial biosystems on a surface. *Acc. Chem. Res.* **47**, 1912–1921 (2014). [Medline doi:10.1021/ar5001428](#)
18. J. Shin, V. Noireaux, Efficient cell-free expression with the endogenous *E. coli* RNA polymerase and sigma factor 70. *J. Biol. Eng.* **4**, 8 (2010). [Medline doi:10.1186/1754-1611-4-8](#)
19. J. Shin, V. Noireaux, An *E. coli* cell-free expression toolbox: Application to synthetic gene circuits and artificial cells. *ACS Synth. Biol.* **1**, 29–41 (2012). [Medline doi:10.1021/sb200016s](#)
20. J. Stricker, S. Cookson, M. R. Bennett, W. H. Mather, L. S. Tsimring, J. Hasty, A fast, robust and tunable synthetic gene oscillator. *Nature* **456**, 516–519 (2008). [Medline doi:10.1038/nature07389](#)
21. J. Shin, V. Noireaux, Study of messenger RNA inactivation and protein degradation in an *Escherichia coli* cell-free expression system. *J. Biol. Eng.* **4**, 9 (2010). [Medline doi:10.1186/1754-1611-4-9](#)
22. L. H. Hartwell, J. J. Hopfield, S. Leibler, A. W. Murray, From molecular to modular cell biology. *Nature* **402** (suppl.), C47–C52 (1999). [Medline doi:10.1038/35011540](#)
23. X. Wang, W. Zeng, G. Lu, O. L. Russo, E. Eisenbraun, High aspect ratio Bosch etching of sub-0.25 μm trenches for hyperintegration applications. *J. Vac. Sci. Technol. B* **25**, 1376 (2007). [doi:10.1116/1.2756554](#)
24. D. Bracha, E. Karzbrun, G. Shemer, P. A. Pincus, R. H. Bar-Ziv, Entropy-driven collective interactions in DNA brushes on a biochip. *Proc. Natl. Acad. Sci. U.S.A.* **110**, 4534–4538 (2013). [Medline doi:10.1073/pnas.1220076110](#)
25. S. S. Daube, D. Bracha, A. Buxboim, R. H. Bar-Ziv, Compartmentalization by directional gene expression. *Proc. Natl. Acad. Sci. U.S.A.* **107**, 2836–2841 (2010). [Medline doi:10.1073/pnas.0908919107](#)
26. E. Karzbrun, J. Shin, R. H. Bar-Ziv, V. Noireaux, Coarse-grained dynamics of protein synthesis in a cell-free system. *Phys. Rev. Lett.* **106**, 048104 (2011). [Medline doi:10.1103/PhysRevLett.106.048104](#)
27. A. E. Karu, Y. Sakaki, H. Echols, S. Linn, The gamma protein specified by bacteriophage gamma. Structure and inhibitory activity for the recBC enzyme of *Escherichia coli*. *J. Biol. Chem.* **250**, 7377–7387 (1975). [Medline](#)